



Thermodynamic investigation of a solar-based multigeneration system using Al_2O_3 -Thermonol VP1 nanofluid

Ahmed Hussein Obaid Ajam | Iraj Mirzaee^{ID} | Samad Jafarmadar*^{ID}
Majid Abbasalizadeh^{ID}

Department of Mechanical Engineering, Faculty of Engineering, Urmia University, Urmia, Iran

* Corresponding author, Email: s.jafarmadar@urmia.ac.ir

Article Information

Article Type

RESEARCH ARTICLE

Article History

RECEIVED: 26 Jul 2024

REVISED: 14 Sep 2024

ACCEPTED: 17 Sep 2024

PUBLISHED ONLINE: 06 Nov 2024

Keywords

Thermodynamic analysis

Nanofluid

Solar collector

Hydrogen

Multigeneration

Abstract

The system underwent a thermodynamic analysis in this research, focusing on the generation of energy, cooling, heating, hydrogen, and freshwater across multiple generations. The primary energy source for this cycle is a solar parabolic trough collector (PTC). In this solar collector, Al_2O_3 Therminol VP1 nanofluid is used as the working fluid. The multigeneration system includes the following subsystems: A steam Rankine cycle and an organic Rankine cycle for power production, a double-effect absorption refrigeration system for cooling, a domestic water heater for hot water generation, a proton exchange membrane (PEM) electrolyzer for hydrogen production, and a reverse osmosis (RO) desalination unit for freshwater production. The ORC cycle will incorporate a thermoelectric generator (TEG) unit instead of a condenser to produce additional power. The system's efficiency is analyzed concerning various factors and nanoparticle concentrations. The findings indicate that the energetic efficiency of the system is 33.81%, while the exergetic efficiency is 23.59%. Additionally, the production rates of hydrogen and freshwater increase with higher nanoparticle volume concentrations and solar irradiation. It was also observed that the coefficient of performance (COP) of the cooling system improves with increasing desorber temperature.

Cite this article: Ajam, A. H. O., Mirzaee, I., Jafarmadar, S., Abbasalizadeh, A. (2024). Thermodynamic investigation of a solar-based multigeneration system using Al_2O_3 -Thermonol VP1 nanofluid. DOI: [10.22104/hfe.2024.6905.1300](https://doi.org/10.22104/hfe.2024.6905.1300)



© The Author(s).

DOI: [10.22104/hfe.2024.6905.1300](https://doi.org/10.22104/hfe.2024.6905.1300)

Publisher: Iranian Research Organization for Science and Technology (IROST)

1 Introduction

Power plants today commonly use fossil fuels to generate heat, which is subsequently converted into electricity. These large power plants typically have an efficiency of about 30 to 35%, meaning that only approximately one-third of the energy from the input fuel is converted into usable energy [1]. Thermal energy can be lost in various ways within these power plants, including through cooling towers, boilers, pumps, and piping systems. Besides, about 15% of the power generated is lost during transmission. This loss can be minimized by generating electricity closer to the point of consumption. To improve energy efficiency, reduce fuel consumption, and lower the cost of primary energy supply, it is crucial to utilize the heat released during the combustion process as much as possible. The waste heat generated by these systems can be effectively utilized for heating, cooling, and various industrial processes [2]. Incorporating combined production of electricity and heat can lead to lower emissions of harmful gases, increased efficiency, and reduced fuel consumption. Combined Heat and Power (CHP) systems utilize the thermal energy generated during power production as a valuable energy source, enhancing overall system efficiency. Industries, hospitals, office buildings, and other facilities that require substantial amounts of thermal energy throughout the day can benefit from employing Combined Heat and Power (CHP) systems to reduce their expenses [3]. A multigeneration system represents an advanced extension of these integrated systems, offering even greater efficiency and utility by simultaneously producing electricity, heating, cooling, and other forms of energy. This category encompasses both cogeneration and trigeneration systems, such as Combined Heat and Power (CHP) systems with CHP technology [4]. Renewable energy sources, such as hydropower and hydrogen, address energy crises and pollutant emissions due to their clean and renewable nature. Integrating Renewable Energy Technology within multigeneration systems appears to be an effective strategy for enhancing energy efficiency and reducing environmental pollutant emissions. In multigeneration systems, solar energy is commonly used as a type of renewables source. Various heat transfer fluids are employed in solar systems, with nanofluids being particularly favored due to their superior heat transfer properties. Researchers have explored multigeneration systems incorporating different prime movers and subsystems to optimize performance and efficiency.

In their study, Godefroy et al. [5] developed, tested, and created a mathematical model for a small-scale trigeneration system. This system integrates a CHP unit,

located at the University of Nottingham in England, with an ejector refrigeration system. The system generates 5.5 kW of power using a reciprocating engine fueled by natural gas. The findings indicate that integrating power, cooling, and heating in a trigeneration system improves overall system efficiency compared to separate production and decreases pollutant emissions. Additionally, the system's efficiency could potentially reach 50%, with further improvements possible by enhancing the refrigeration system's performance, particularly through increasing the steam generator's temperature.

In a proposal, Khaliq [6] suggested a trigeneration system powered by a gas turbine to simultaneously generate power, heat, and cooling. The system includes a gas turbine, combustion chamber, compressor, absorption chiller, and steam generator. Upon analyzing the exergy degradation of different components, it was found that the combustion chamber and steam generator are the primary contributors, accounting for 80% of the total exergy degradation. This contribution increases with higher turbine inlet temperatures and decreases as the pressure ratio increases.

Al-Sulaiman et al. [7] explored the solar trigeneration system from the exergy perspective, analyzing power, cooling, and heating in three different modes:

1. Sole utilization of solar energy.
2. Utilization of solar energy combined with a storage source.
3. Sole utilization of the storage source.

This system comprises an organic Rankine cycle, an absorption refrigeration subsystem, a solar collector, and a storage source, utilizing octane as the working fluid due to its high critical temperature. The analysis revealed that the solar collector and evaporators are major contributors to exergy destruction, highlighting the importance of careful design and selection of these components. Furthermore, the maximum exergy performance was found to be 20% in the first operating mode, 8% in the second mode, and 7% in the third mode. In their study, Boyaghchi and Heidarnejad [8] analyzed and optimized the exergy of a triple solar production system based on the Organic Rankine Cycle (ORC). They first developed a model of the system's exergy for both winter and summer seasons. Subsequently, they assessed the sensitivity of the system with respect to various design parameters, including turbine inlet pressure and temperature, turbine outlet pressure, mass flow rate through the turbine, and collector surface area. By maximizing thermal efficiency and exergy, there was a 4.63% increase in summer and a 46.36% increase in winter for thermal efficiency. Similarly, exergy increased by 2.95% in summer and 47.1% in winter.

In their study, Wang et al. [9] analyzed the thermodynamic efficiency and improvement of a combined heat, power, and cooling (CCHP) system configuration, along with its integration with solar energy and natural gas. The arrangement includes a unit for generating power, a system for recovering heat, a system for absorption cooling, and a storage tank, all combined with PV panels and a vacuum tube thermal collector. Through thermodynamic analyzing, the researchers explored the system's energy efficiency and exergy under various operating conditions. The findings revealed that integrating photovoltaic (PV) panels with the CCHP system enhanced exergy efficiency, while incorporating the solar thermal collector improved energy efficiency. Abid et al. [10] conducted a comparative study examining the integration of trough solar collectors and parabolic dish solar collectors with a Rankine cycle and an electrolyzer for power and hydrogen generation. The findings indicate that, in comparison to the parabolic trough's net power production of 1 kW–6.23 kW, the parabolic dish assisted thermal plant achieves a higher net power output of 2.45 kW to 8.17 kW. The nanofluids, particularly those based on aluminum oxide (Al_2O_3) and ferrosilicon (Fe_2O_3), exhibit greater efficiency and net energy when compared to lump salts. Additionally, the parabolic trough thermal power plant produces hydrogen at a rate between 0.00395 g/s and 0.02454 g/s, whereas the parabolic dish thermal power plant generates hydrogen at a rate ranging from 0.0098 g/s to 0.0322 g/s.

Ibrahim et al. [11] have introduced an innovative multigeneration setup comprising compound parabolic collectors and a biomass combustion unit. The system involves multiple components, including an organic Rankine cycle, a double-stage refrigeration system, a dryer, a steam Rankine cycle, a multistage flash distillation system, and a proton exchange membrane electrolyzer. To harness fluids in the Solar Cycle, graphene and silver nanoparticles with distinct high-quality properties were selected to be used with ethylene glycol. The findings indicate that the overall system performance benefited from increased solar irradiation, environmental temperature, exit temperatures of biomass combustors, and nanofluid concentrations. Furthermore, the application of nanofluids as working fluids in solar collectors led to evident enhancements in system performance.

Pourmoghadam and Kasaeian [12] utilized EES, MATLAB and TRNSYS software to model the dynamic operation of a solar system for combined heating, cooling, water production and power generation. The initial scenario led to LCOW, LCOE, LCOC, and LCOH values of 2.984 dollars per cubic meter, 0.121 dollars per kilowatt hour, 0.064 dollars per kilowatt

hour, and 0.019 dollars per kilowatt hour, respectively. Additionally, a repayment period of six years was determined for the base case.

An analysis of previous research indicates that numerous studies have focused on solar multigeneration systems. However, there has been limited exploration of the utilization of nanofluids in solar collectors. Additionally, the use of a TEG unit for enhancing power generation has not been widely implemented in multigeneration systems. Consequently, this thesis focuses on the implementation of a solar-based multigeneration system designed to yield multiple outputs. The primary outputs of the system include power, heating, cooling, hydrogen, fresh water, and hot water. The objective of employing solar power is to contribute to the reduction of greenhouse gas emissions and decrease reliance on fossil fuels. Nanofluids are incorporated into the solar collector to augment heat transfer. Furthermore, a TEG unit is integrated into the ORC cycle to elevate the system's power generation capacity.

2 System description

Figure 1 illustrates the diagram of the system under study. The primary energy source of the system is the solar collector. The steam Rankine cycle, the ORC cycle and the TEG unit are responsible of producing power. The double-effect absorption refrigeration cycle produces the cooling effect, while hot water is supplied by the domestic water heater. Hydrogen is generated in the PEM electrolyzer, and freshwater is produced by the RO water desalination unit. Solar energy in this setup is gathered using a parabolic solar collector. The operating fluid used in the collector is Al_2O_3 -Therminol VP1 nanofluid. After absorbing heat from the PTC solar collector, the working fluid becomes hot and is then transferred to the hot storage tank at point 1. This stored heat can be utilized when sunlight is insufficient. After passing through the storage tank, the fluid reaches point 2 and flows through the steam generator of the steam Rankine cycle to heat the cycle's working fluid. After passing through the steam generator, the working fluid is used to heat water at point 3, maximizing the utilization of the remaining energy. At point 4, the fluid then enters the double-effect absorption chiller generator for cooling purposes. Following this, at point 5, it enters the storage tank, and finally, at point 6, it is pumped back towards the collector. In the steam Rankine cycle or ORC cycle, the working fluid, which starts as a saturated liquid, is pumped by the pump to the inlet pressure of the turbine. The fluid is then expanded in the turbine to generate mechanical energy.

$$\dot{C}_{p,tot} = \dot{C}_{F,tot} + \dot{Z}_{tot}^{CI} + \dot{Z}_{tot}^{O\&M}, \quad (5)$$

$$\dot{Z}_k = \frac{Z_k \varphi CRF}{\tau}, \quad (6)$$

$$CRF = \frac{i_r(1 + i_r)^n}{(1 + i_r)^n - 1}. \quad (7)$$

In the cost rate equation (\dot{Z}_k), Z_k represents the cost per component, φ represents the maintenance factor, which is 1.06, and N is the number of operating hours of the system. In the capital recovery factor (CRF) equation, i and n represent the interest rate and the lifetime of the system, respectively, with values of 0.1 and 20.

Some general assumptions are stated below:

- The system operates at a constant state.
- Pressure drop in the evaporator, condenser, steam generator, and all heat exchangers is not considered.
- The condenser produces fluid in the state of saturated liquid at its exit.
- Pump and turbine performance follow the isentropic process.
- All components studied in the system are considered as control volumes.
- Uniform and constant solar radiation is assumed.

The PTC solar collector in this study uses nanofluid as the working fluid, which consists of Therminol VP1 as the base fluid and Al_2O_3 as the nanoparticle. [Table 1](#) presents the thermodynamic characteristics of the nanoparticles.

Table 1. Characteristics of studied nanoparticles [17].

Material	k (W/m.K)	ρ (kg/m ³)	c_p (kJ/kgK)
Al_2O_3	40	3970	0.765

The nanofluid’s thermophysical properties are as follows [18–20]:

$$\rho_{nf} = \varphi \rho_{np} + (1 - \varphi) \rho, \quad (8)$$

$$c_{p,nf} = \frac{\rho_{np} \varphi c_{p,np} + \rho(1 - \varphi) c_p}{\rho_{nf}}, \quad (9)$$

$$k_{nf} = k \frac{k_{np} + 2k + 2(k_{np} - k)(1 + \beta)^3 \varphi}{k_{np} + 2k - (k_{np} - k)(1 + \beta)^3 \varphi}, \quad (10)$$

$$\mu_{nf} = \mu(1 + 2.5 \varphi + 6.5 \varphi^2), \quad (11)$$

The exergy loss rate and the financial equilibrium equations for each element can be computed using the energy and exergy balance equations for a potential multi-generation system, as illustrated in [Table 2](#).

Table 2. Equations of exergy destruction rate for each component of the proposed system.

Component	Energy balance equations	Exergy destruction rate equations
PTC collector	$\dot{m}_7 h_7 + \dot{Q}_u = \dot{m}_1 h_1$	$\dot{E}x_{D,PTC} = \dot{E}x_{sun} + \dot{E}x_7 - \dot{E}x_1$
Hot storage	$\dot{Q}_{hs} = U(T_1 - T_0)$	$\dot{E}x_{d,hs} = \dot{E}x_1 - \dot{E}x_2 - \dot{E}x_Q$
DWH	$\dot{Q}_{DWH} = \dot{m}_3(h_3 - h_4) = \dot{m}_8(h_9 - h_8)$	$\dot{E}x_{DWH} = \dot{E}x_3 + \dot{E}x_8 - \dot{E}x_4 - \dot{E}x_9$
Warm storage	$\dot{Q}_{ws} = U(T_5 - T_0)$	$\dot{E}x_{d,ws} = \dot{E}x_5 - \dot{E}x_6 - \dot{E}x_{Q,ws}$
Steam generator	$\dot{Q}_{sg,src} = \dot{m}_2(h_2 - h_3) = \dot{m}_{10}(h_{10} - h_{13})$	$\dot{E}x_{D,sg,src} = \dot{E}x_2 + \dot{E}x_{13} - \dot{E}x_3 - \dot{E}x_{10}$
SRC turbine	$\dot{W}_{t,src} = \dot{m}_{10}(h_{10} - h_{11})$	$\dot{E}x_{D,t,src} = \dot{E}x_{10} - \dot{W}_{t,src} - \dot{E}x_{11}$
SRC heat exchanger	$\dot{Q}_{hx,src} = \dot{m}_{11}(h_{11} - h_{12}) = \dot{m}_{14}(h_{14} - h_{22})$	$\dot{E}x_{D,hx,src} = \dot{E}x_{11} + \dot{E}x_{22} - \dot{E}x_{12} - \dot{E}x_{14}$
ORC turbine	$\dot{W}_{t,orc} = \dot{m}_{14}(h_{14} - h_{15}) + \dot{m}_{16}(h_{16} - h_{15})$	$\dot{E}x_{D,t,orc} = \dot{E}x_{14} - \dot{W}_{t,orc} - \dot{E}x_{15} - \dot{E}x_{16}$
ORC TEG	$\dot{Q}_{TEG,orc} = \dot{m}_{17}(h_{17} - h_{18}) = \dot{m}_{23}(h_{24} - h_{23})$	$\dot{E}x_{D,TEG,orc} = \dot{E}x_{17} + \dot{E}x_{23} - \dot{E}x_{18} - \dot{E}x_{24}$
ORC Pump 1	$\dot{W}_{p1,orc} = \dot{m}_{18}(h_{19} - h_{18})$	$\dot{E}x_{D,p1,orc} = \dot{W}_{p1,orc} - \dot{E}x_{18} + \dot{E}x_{19}$
ORC Pump 2	$\dot{W}_{p2,orc} = \dot{m}_{21}(h_{22} - h_{21})$	$\dot{E}x_{D,p2,orc} = \dot{W}_{p2,orc} - \dot{E}x_{21} + \dot{E}x_{22}$
ORC IHE	$\dot{Q}_{IHE,orc} = \dot{m}_{16}(h_{16} - h_{17}) = \dot{m}_{19}(h_{20} - h_{19})$	$\dot{E}x_{D,IHE,orc} = \dot{E}x_{16} + \dot{E}x_{19} - \dot{E}x_{17} - \dot{E}x_{20}$
ORC OFOH	–	$\dot{E}x_{D,OFOH,orc} = \dot{E}x_{20} + \dot{E}x_{15} - \dot{E}x_{21}$
DEARC-High desorber	$\dot{Q}_{Hdes,DEARC} = \dot{m}_4(h_4 - h_5)$	$\dot{E}x_{d,DEARC,Hdes} = \dot{E}x_4 + \dot{E}x_{37} - \dot{E}x_5 - \dot{E}x_{38} - \dot{E}x_{41}$
DEARC-High condenser	$\dot{Q}_{Hcond,DEARC} = \dot{m}_{41}(h_{41} - h_{42})$	$\dot{E}x_{d,Hcond,DEARC} = \dot{E}x_{41} - \dot{E}x_{42}$

Table 2. Equations of exergy destruction rate for each component of the proposed system (Continued).

Component	Energy balance equations	Exergy destruction rate equations
DEARC-Solution heat exchanger 1	$\dot{Q}_{\text{SHX1,DEARC}} = \dot{m}_{28}(h_{28} - h_{29}) = \dot{m}_{26}(h_{27} - h_{26})$	$\dot{E}x_{d,\text{SHX1,DEARC}} = \dot{E}x_{26} + \dot{E}x_{28} - \dot{E}x_{27} - \dot{E}x_{29}$
DEARC-Solution heat exchanger 2	$\dot{Q}_{\text{SHX2,DEARC}} = \dot{m}_{38}(h_{38} - h_{39}) = \dot{m}_{36}(h_{37} - h_{36})$	$\dot{E}x_{d,\text{SHX2,DEARC}} = \dot{E}x_{36} + \dot{E}x_{38} - \dot{E}x_{37} - \dot{E}x_{39}$
DEARC-Low condenser	$\dot{Q}_{\text{Lcond,DEARC}} = \dot{m}_{31}h_{31} + \dot{m}_{43}h_{43} - \dot{m}_{32}h_{32} = \dot{m}_{44}(h_{45} - h_{44})$	$\dot{E}x_{d,\text{Lcond,DEARC}} = \dot{E}x_{31} + \dot{E}x_{43} + \dot{E}x_{44} - \dot{E}x_{32} - \dot{E}x_{45}$
DEARC-Evaporator	$\dot{Q}_{\text{eva,DEARC}} = \dot{m}_{34}(h_{34} - h_{33}) = \dot{m}_{48}(h_{49} - h_{48})$	$\dot{E}x_{d,\text{eva,DEARC}} = \dot{E}x_{33} + \dot{E}x_{48} - \dot{E}x_{34} - \dot{E}x_{49}$
DEARC-Absorber	$\dot{Q}_{\text{abs,DEARC}} = \dot{m}_{34}h_{34} + \dot{m}_{30}h_{30} - \dot{m}_{25}h_{25} = \dot{m}_{46}(h_{47} - h_{46})$	$\dot{E}x_{d,\text{abs,DEARC}} = \dot{E}x_{34} + \dot{E}x_{30} + \dot{E}x_{46} - \dot{E}x_{25} - \dot{E}x_{47}$
DEARC-Pump 1	$\dot{W}_{p1,\text{DEARC}} = \dot{m}_{25}(h_{26} - h_{25})$	$\dot{E}x_{d,p1,\text{DEARC}} = \dot{W}_{p1,\text{DEARC}} + \dot{E}x_{25} - \dot{E}x_{26}$
DEARC-Pump 2	$\dot{W}_{p2,\text{DEARC}} = \dot{m}_{35}(h_{36} - h_{35})$	$\dot{E}x_{d,p2,\text{DEARC}} = \dot{W}_{p2,\text{DEARC}} + \dot{E}x_{35} - \dot{E}x_{36}$
PEM	$\dot{W}_{\text{PEM}} = \dot{m}_9h_9 - \dot{m}_{53}h_{53} - \dot{m}_{54}h_{54}$	$\dot{E}x_{D,\text{PEM}} = \dot{E}x_9 + \dot{W}_{\text{PEM}} - \dot{E}x_{53} - \dot{E}x_{54}$
RO	$\dot{W}_{\text{RO}} = \dot{m}_{50}h_{50} - \dot{m}_{51}h_{51} - \dot{m}_{52}h_{52}$	$\dot{E}x_{D,\text{RO}} = \dot{E}x_{50} - \dot{E}x_{51} - \dot{E}x_{52}$
COP	$\text{COP} = \frac{\dot{Q}_{\text{eva,DEARC}}}{\dot{Q}_{\text{Hdes,DEARC}} + \dot{W}_{\text{net,DEARC}}}$	
Energy efficiency	$\eta_{\text{th,tot}} = \frac{\dot{W}_{\text{SRC}} + \dot{W}_{\text{ORC}} + \dot{W}_{\text{TEG}} + \dot{Q}_{\text{cooling}} + \dot{Q}_{\text{DWH}} + \dot{m}_{53}\text{HHV}_{\text{H}_2} - \dot{W}_{\text{PEM}} + \dot{m}_{51}h_{51} - \dot{W}_{\text{RO}}}{\dot{Q}_u}$	
Exergy efficiency	$\eta_{\text{ex,tot}} = \frac{\dot{W}_{\text{SRC}} + \dot{W}_{\text{ORC}} + \dot{W}_{\text{TEG}} + \dot{E}x_{\text{cooling}} + \dot{E}x_{53} + \dot{E}x_{54} + \dot{E}x_{51} + \dot{E}x_9}{\dot{E}x_{\text{in,sun}}}$	

4 Results and discussion

The proposed system is new and has not been previously tested, resulting in insufficient data for verification. Reference [21] has been used to compare certain components of the system, with the comparison results presented in Table 3 for validation and code verification. The model demonstrates proper validity, as evidenced by the results, confirming that the written code has been validated.

Table 3. Comparison of the findings in the current study with those of Jang and Lee [21].

Parameter	Unit	This study	Ref [21]	Difference (%)
\dot{W}_i	kW	2.03	2.03	0
\dot{Q}_{eva}	kW	32.74	33.54	0.61
\dot{Q}_{con}	kW	26.51	26.51	0
η_{ORC}	%	5.96	6.04	1.32
H_{CHP}	%	72.14	72.26	0.16

To model the multigeneration system, some initial assumptions are required. The basic assumptions con-

sidered for the system simulation are presented in the Table 4. The outcomes of the analyzed system following the simulation are displayed in Table 5.

Figure 2 illustrates the exergy destruction rates in the primary components of the system under study. The graphs clearly show that the PTC collector and the organic Rankine cycle exhibit the highest rates of exergy loss. In solar systems, a significant portion of solar radiation exergy is dissipated into the environment as thermal waste from solar collectors. The substantial temperature differential between the fluid entering the panel and its surface temperature is a key factor contributing to the elevated exergy destruction rate in these systems. Figure 3 displays a comparison of four different working fluids in terms of hydrogen and freshwater production rates. The results indicate that n-pentane has the highest hydrogen production rate among the fluids studied. The high hydrogen production rate observed with n-pentane is due to the greater amount of power generated by the ORC cycle when using this fluid. The results also show equal freshwater generation rates across all working fluids. This is because the power supplied to the RO unit comes from the SRC cycle, so the choice of ORC working fluid does not affect the freshwater production rate.

Table 4. Input parameters for the modeling of the present study [22–27].

Parameters	Unit	Value
Collector width, w	m	5.76
Collector length, L	m	12.27
Receiver outside diameter, $D_{o,r}$	m	0.07
Receiver inside diameter, $D_{i,r}$	m	0.066
Receiver inlet temperature, T_{ri}	°C	100
Solar radiation intensity, G_b	W/m ²	850
Recovery ratio, RR	–	0.3
Number of elements, n_e	–	7
Number of pressure vessels, n_v	–	42
Seawater salinity, X_f	g/kg	43
Turbine inlet pressure, P_{10}	kPa	2500
Turbine outlet pressure, P_{12}	kPa	100
Turbine inlet temperature, T_{14}	°C	140
Turbine pressure ratio	–	5
Pump inlet temperature, T_{18}	°C	40
Turbine isentropic efficiency, $\eta_{t,ORC}$	%	85
Pump isentropic efficiency, $\eta_{p,ORC}$	%	80
P_{H_2}, P_{O_2}	atm	1
T_{PEM}	°C	80
$E_{act,a}$	kJ/mol	76
$E_{act,c}$	kJ/mol	18
λ_a	–	14
λ_c	–	10
D	mm	50
J_a^{ref}	A/m ²	1.7×10^5
J_c^{ref}	A/m ²	4.6×10^3
Evaporator temperature, T_{eva}	°C	5
Condenser temperature, T_{con}	°C	35
Absorber temperature, T_{abs}	°C	35
Desorber temperature, T_{des}	°C	100
SHX	%	80

Table 5. The general simulation results for the proposed system.

Parameters	Unit	Value
η_{en}	%	33.81
η_{ex}	%	23.59
Q_u	kW	11406
$\dot{W}_{t,SRC}$	kW	1526
$\dot{W}_{t,ORC}$	kW	328.9
\dot{W}_{TEG}	kW	226.6
COP	–	1.071
$Q_{cooling}$	kW	165
\dot{m}_{H_2}	kg/day	235.1
$\dot{m}_{freshwater}$	kg/s	4.99
$\dot{E}x_{d,tot}$	kW	53191

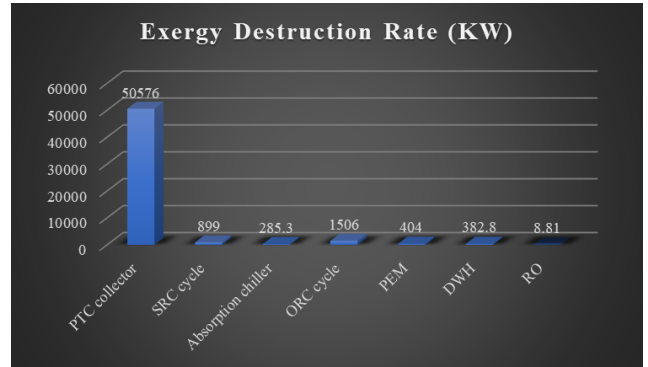
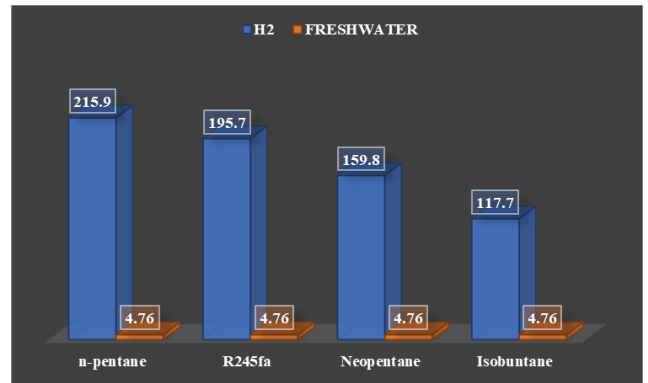
**Fig. 2.** Exergy destruction rate for the main equipment of the studied cycle.**Fig. 3.** Comparison of four different working fluids in terms of hydrogen and freshwater generation rates.

Figure 4 illustrates the impact of nanoparticle volume concentration on the hydrogen and freshwater generation rates of the system. The graphs show a direct correlation, with increases in nanoparticle volume concentration leading to higher rates of both hydrogen and freshwater generation. As the volume concentration increases from 0 to 0.1, the hydrogen generation rate rises from 215.9 kg/day to 252.3 kg/day, and the freshwater generation rate increases from 4.767 kg/s to 5.192 kg/s. This enhancement in both hydrogen and freshwater generation rates is attributed to the increased total power produced by the SRC and ORC systems as a result of the higher nanoparticle volume concentration.

Figure 5 shows the influence of solar radiation on the hydrogen production rate at different volume concentrations. The PEM electrolyzer is fed by both the ORC cycle turbine and the TEG unit. The data reveal that, for all volume concentrations, the hydrogen generation rate increases with rising solar irradiation. Furthermore, for a given level of solar radiation, higher nanoparticle volume concentrations result in greater hydrogen production by the system for a solar radiation level of 700 W/m², the hydrogen generation rate

is 162.4 kg/day without nanoparticles, whereas it increases to 187.9 kg/day with a nanoparticle volume concentration of 0.1. This improvement is due to the reduced specific heat of the nanofluid at higher volume concentrations, which means less energy is required to heat the working fluid. Consequently, the output temperatures of the PTC increase, leading to more power being generated by the Rankine cycle and the TEG unit. This results in a greater energy supply to the electrolyzer, enhancing hydrogen production.

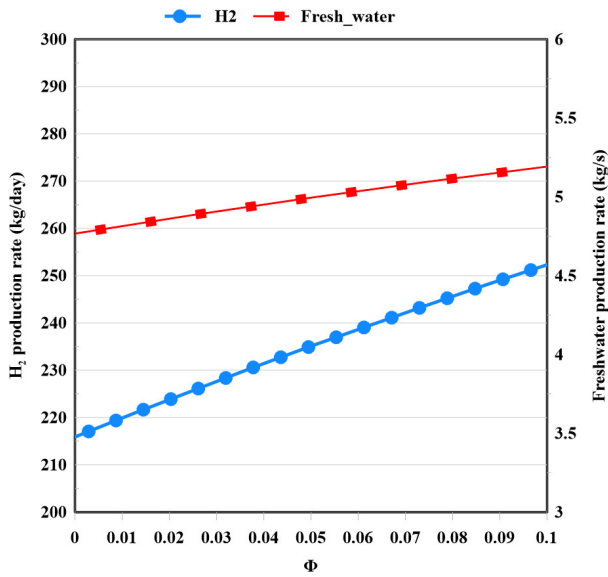


Fig. 4. The effect of nanoparticle volume concentration on the hydrogen and freshwater generation rates of the system.

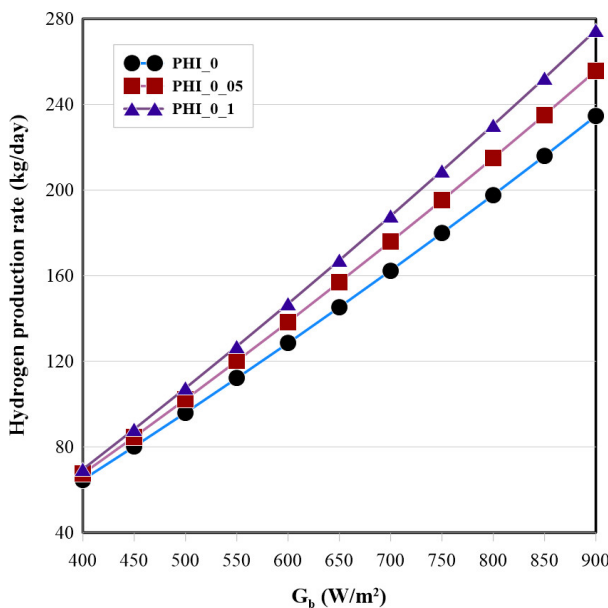


Fig. 5. Impact of solar radiation on the hydrogen generation rate at different volume concentrations.

Figure 6 illustrates the impact of nanoparticle concentration and solar radiation on the overall performance of the multi-generation system. Increased solar radiation improves both energy and exergy efficiency by enhancing heat transfer into the PTC’s working fluid, which raises its output temperature. Consequently, this increase in the input steam temperature for the Rankine cycle leads to greater power generation, with excess power being transferred to the ORC cycle by the SRC cycle. Thus, higher solar radiation results in enhanced energy and exergy efficiency. Additionally, increasing the volume fraction of nanoparticles also improves energy and exergy efficiencies. This improvement is due to the higher nanoparticle concentration, which increases the nanofluid density and reduces its heat capacity, allowing the collector to absorb more heat. As a result, the Rankine cycles receive more power, leading to increased electricity production. The surplus power also benefits the PEM electrolyzer and RO unit, enhancing hydrogen production and freshwater generation. Additionally, the double-effect absorption refrigeration system utilizes a portion of the PTC’s heat energy to improve its cooling performance. Therefore, higher volume fractions of nanoparticles contribute to increased overall energy and exergy efficiency, with greater nanoparticle concentrations yielding improved energetic and exergetic performance.

Figure 7 illustrates the effect of a high desorber temperature on the system’s coefficient of performance (COP). The graph shows a slight increase in COP up to a peak, followed by stabilization as the desorber temperature rises significantly. Increasing the desorber temperature leads to higher temperatures for both the refrigerant and the solution as they exit the desorber. Specifically, as the high desorber temperature increases from 363 K to 403 K, the COP of the system increases from 0.93 to 1.07.

5 Conclusions

This study analyzed a multi-generation system that produces electricity, cooling, domestic heating, hydrogen, and freshwater through a thermodynamic analysis. The solar PTC collector serves as the primary energy source for the system. Al₂O₃-Therminol VP1 nanofluid is used as the working fluid for the solar collector. The system is analyzed with the help of EES software, considering the impact of various parameters on its performance. The primary conclusions of the study are as follows: The system’s energy efficiency is 33.81%, while its exergy efficiency is 23.89%. The additional power of 226.6 kW can be achieved by replacing the ORC condenser with a TEG unit.

It can produce 235.1 kg of hydrogen per day and 4.99 kg of freshwater per day through this multigeneration system.

In terms of exergy destruction, the PTC solar collectors and ORC cycles exhibit the highest levels.

The rates of hydrogen and freshwater production increase with higher nanoparticle volume concentrations.

Increasing in solar radiation leads to higher energetic and exergetic efficiency, as well as an increased rate of hydrogen production in the system under study.

As the high desorber temperature increases, the COP of the system rises.

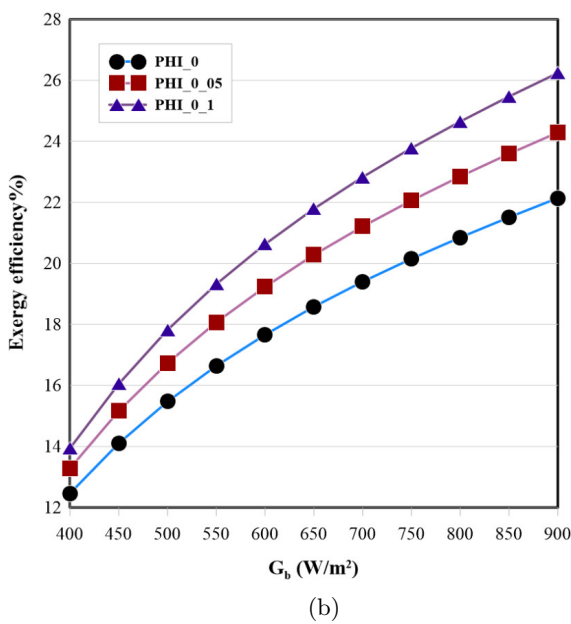
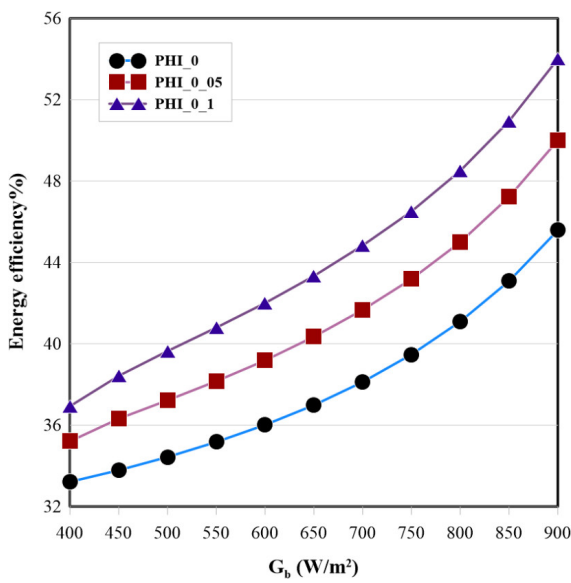


Fig. 6. Impact of solar radiation on the energy and exergy efficiency at different volume concentrations.

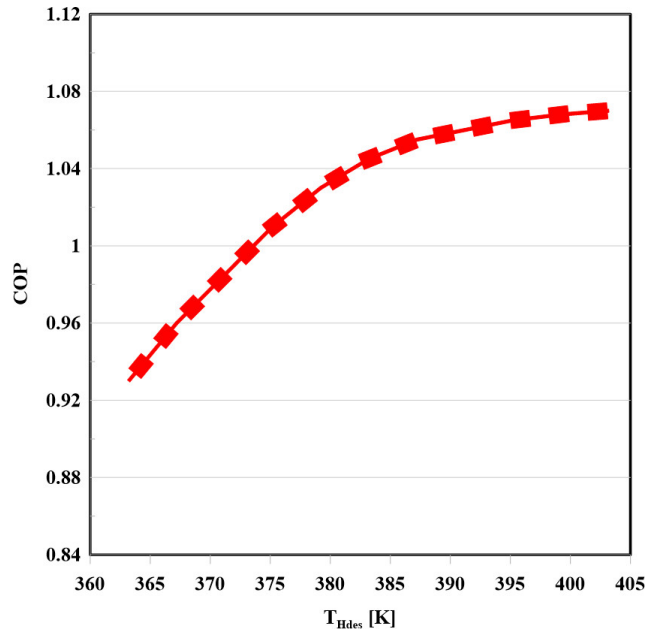


Fig. 7. Impact of high desorber temperature on the COP.

References

- [1] Chaplin RA. Thermal power plants. Encyclopedia of Life Support Systems; 2009. 238
- [2] Jouhara H, Khordehghah N, Almahmoud S, Delpach B, Chauhan A, Tassou SA. Waste heat recovery technologies and applications. Thermal Science and Engineering Progress. 2018;6:268–289. 238
- [3] Bradford T. Solar revolution: the economic transformation of the global energy industry. MIT Press; 2008. 238
- [4] Dincer I, Zamfirescu C. Advanced power generation systems. Academic Press; 2014. 238
- [5] Godefroy J, Boukhanouf R, Riffat S. Design, testing and mathematical modelling of a small-scale CHP and cooling system (small CHP-ejector trigeneration). Applied Thermal Engineering. 2007;27(1):68–77. 238
- [6] Khaliq A. Exergy analysis of gas turbine trigeneration system for combined production of power heat and refrigeration. International Journal of Refrigeration. 2009;32(3):534–545. 238
- [7] Al-Sulaiman FA, Dincer I, Hamdullahpur F. Exergy modeling of a new solar driven trigeneration system. Solar Energy. 2011;85(9):2228–2243. 238

- [8] Boyaghchi FA, Heidarnajad P. Thermodynamic analysis and optimisation of a solar combined cooling, heating and power system for a domestic application. *International journal of exergy*. 2015;16(2):139–168. [238](#)
- [9] Wang J, Lu Y, Yang Y, Mao T. Thermodynamic performance analysis and optimization of a solar-assisted combined cooling, heating and power system. *Energy*. 2016;115:49–59. [239](#)
- [10] Abid M, Ratlamwala TA, Atikol U. Solar assisted multi-generation system using nanofluids: a comparative analysis. *International Journal of Hydrogen Energy*. 2017;42(33):21429–21442. [239](#)
- [11] Ibrahim AA, Kayfeci M, Georgiev AG, Dolgun GK, Keçebaş A. Performance Assessment of a Novel Solar and Biomass-Based Multi-Generation System Equipped with Nanofluid-Based Compound Parabolic Collectors. *Energies*. 2022;15(23):8911. [239](#)
- [12] Pourmoghadam P, Kasaeian A. Economic and energy evaluation of a solar multi-generation system powered by the parabolic trough collectors. *Energy*. 2023;262:125362. [239](#)
- [13] Çengel YA, Boles MA, Kanoğlu M. *Thermodynamics: An Engineering Approach*. McGraw-Hill; 2011. [240](#)
- [14] Mokhtari H, Esmaili A, Hajabdollahi H. Thermo-economic analysis and multiobjective optimization of dual pressure combined cycle power plant with supplementary firing. *Heat Transfer—Asian Research*. 2016;45(1):59–84. [240](#)
- [15] Khanmohammadi S, Atashkari K, Kouhikamali R. Exergoeconomic multi-objective optimization of an externally fired gas turbine integrated with a biomass gasifier. *Applied Thermal Engineering*. 2015;91:848–859. [240](#)
- [16] Aras H, Balli O. Exergoeconomic analysis of a combined heat and power system with the micro gas turbine (MGTCHP). *Energy Exploration & Exploitation*. 2008;26(1):53–70. [240](#)
- [17] Duangthongsuk W, Wongwises S. An experimental study on the heat transfer performance and pressure drop of TiO₂-water nanofluids flowing under a turbulent flow regime. *International journal of heat and mass transfer*. 2010;53(1-3):334–344. [241](#)
- [18] Ghasemi SE, Ranjbar AA. Thermal performance analysis of solar parabolic trough collector using nanofluid as working fluid: A CFD modelling study. *Journal of Molecular Liquids*. 2016;222:159–166. [241](#)
- [19] Kasaeian AB. Convection heat transfer modeling of Ag nanofluid using different viscosity theories. *IIUM Engineering Journal*. 2012;13(1). [241](#)
- [20] Khanafer K, Vafai K. A critical synthesis of thermophysical characteristics of nanofluids. In: *Nanotechnology and energy*. Jenny Stanford Publishing; 2017. p. 279–332. [241](#)
- [21] Jang Y, Lee J. Optimizations of the organic Rankine cycle-based domestic CHP using biomass fuel. *Energy Conversion and Management*. 2018;160:31–47. [242](#)
- [22] Al-Sulaiman FA. Exergy analysis of parabolic trough solar collectors integrated with combined steam and organic Rankine cycles. *Energy Conversion and Management*. 2014;77:441–449. [243](#)
- [23] Nafey A, Sharaf M. Combined solar organic Rankine cycle with reverse osmosis desalination process: energy, exergy, and cost evaluations. *Renewable Energy*. 2010;35(11):2571–2580. [243](#)
- [24] Mohammadi M, Mahmoudan A, Nojedehi P, Hoseinzadeh S, Fathali M, Garcia DA. Thermo-economic assessment and optimization of a multi-generation system powered by geothermal and solar energy. *Applied Thermal Engineering*. 2023;230:120656. [243](#)
- [25] Tekkanat B, Yuksel YE, Ozturk M. The evaluation of hydrogen production via a geothermal-based multigeneration system with 3E analysis and multi-objective optimization. *International Journal of Hydrogen Energy*. 2023;48(22):8002–8021. [243](#)
- [26] Sabbaghi MA, Soltani M, Rosen MA. A comprehensive 6E analysis of a novel multigeneration system powered by solar-biomass energies. *Energy*. 2024;297:131209. [243](#)
- [27] Kaynakli O, Saka K, Kaynakli F. Energy and exergy analysis of a double effect absorption refrigeration system based on different heat sources. *Energy Conversion and Management*. 2015;106:21–30. [243](#)